Exact Solution for Elastic Networks on Curved Surfaces

Yinan Dong● and Roya Zandi

Department of Physics and Astronomy, University of California, Riverside, Riverside, California 92521, USA

Alex Travesset

Department of Physics and Astronomy, Iowa State University and Ames Lab, Ames, Iowa 50011, USA

The problem of characterizing the structure of an elastic network constrained to lie on a frozen curved surface appears in many areas of science and has been addressed by many different approaches, most notably, extending linear elasticity or through effective defect interaction models. In this Letter, we show that the problem can be solved by considering nonlinear elasticity in an exact form without resorting to any approximation in terms of geometric quantities. In this way, we are able to consider different effects that have been unwieldy or not viable to include in the past, such as a finite line tension, explicit dependence on the Poisson ratio, or the determination of the particle positions for the entire lattice. Several geometries with rotational symmetry are solved explicitly. Comparison with linear elasticity reveals an agreement that extends beyond its strict range of applicability. Implications for the problem of the characterization of virus assembly are also discussed.

Deciphering the design principles of life is one of the lingering mysteries facing researchers in many areas of science. Among many biological systems, viruses, in particular, have received much more attention as they are ubiquitous pathogens in our environment with members infecting all kingdoms of life. Most viruses, from the simplest to the most complicated, and from the least to the most evolved, are constituted of a protein shell (or "capsid") that encloses the viral genetic material (RNA or DNA) [1,2]. Understanding the process of virus assembly is a fundamental challenge of ever-increasing interest, not only because it is a central stage of the viral life cycle, but also because it is the target of antiviral therapeutic strategies. The coronavirus disease 2019 (COVID-19) pandemic, connected to SARS-CoV-2 revealed more than ever the importance of identifying new ways to combat viruses. In this context, our current understanding of virus assembly is quite limited. The difficulties arise from the interplay between curvature and crystalline order and their role in determining the positions of lattice defects on elastic surfaces with nonzero Gaussian curvature [3–6].

Figure 1 illustrates the structure of two viruses with different geometries: (a) herpes simplex virus (HSV) with icosahedral symmetry [7] and (b) human immuno-deficiency virus (HIV) [8] with a conical structure. In the case of HSV, the position of 12 pentagonal defects is precise [Fig. 1(c)] to preserve the symmetry of the shell. In previous work, we have shown that as a triangular lattice such as a HSV shell [Fig. 1(c)] [9] grows over a spherical scaffold, defects appear one by one at the vertices of an icosahedron, explaining how error-free structures with icosahedral order assemble. For HIV shells, while there
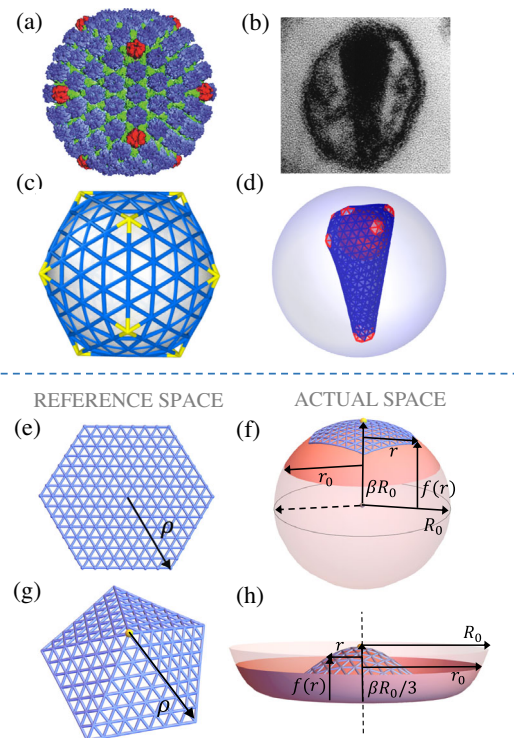

FIG. 1. (a) 3D cryo-EM (electron microscopy) reconstruction of HSV [7]; (b) EM image of HIV surrounded with the lipid envelope [8]. The result of the computer simulations of (c) a HSV [9] and (d) a HIV with genome and membrane [10]. (e) The reference space consists of a flat surface without a disclination or (g) with a disclination at the center. The actual space is any manifold endowed with its natural metric. As an example, we consider (f) a spheroid ($\beta = 1$) and (h) a sombrero ($\beta = 3$).

are often 5 defects at the smaller and 7 at the larger caps, defect positions can vary from one HIV structure to another. The computer simulations of Ref. [10] have shown how the presence of genome and membrane contributes to the formation of the conspicuous conical HIV structures; nevertheless, currently, there is no clear understanding of what determines the position of the defects as the surfaces with nonzero Gaussian curvature such as the conical shell of HIV grow.

Capsid formation dynamics is just one example of the more general class of problems consisting of crystal growth on curved geometries. Other examples are faceted insect eyes, liquid crystals, curved array of microlenses in optical engineering systems, other protein cages in addition to viral capsids such as platonic hydrocarbons, heat shock proteins, ferritins, carboxysomes, silicages, multicomponent ligand assemblies, clathrin vesicles, and many other cellular organelles, as reviewed in Ref. [11], for example. These problems have been mostly addressed by extending linear elasticity [12–17] or through effective defect interaction models [18–23]. Either approach brings significant limitations: linear elasticity and its extensions impose certain approximations on geometric quantities such as Gaussian curvature [see discussion in the Supplemental Material (SM) Sec. III [24], specially Eq. (S20)] and fail to satisfy global topological and geometrical constraints, most notably the Gauss-Bonnet theorem [25]. Effective defect interaction models satisfy global properties exactly, but with uncontrolled approximations and obvious deficiencies: they predict a universal independence of all measurable quantities on the Poisson ratio ν_p and it is unknown, thus far, how to include other relevant free energy terms such as line tension. Furthermore, it requires computing the inverse square Laplacian, a formidable complex task beyond simple cases.

In this Letter, we formulate general elasticity in curved surfaces based on geometric invariants and solve the equations exactly. We build upon our previous results for spherical caps [25,26] combined with covariant elasticity [27,28]. Thus, the approach not only surmounts all the limitations of the previous theories, but provides an exact solution to the problem. Furthermore the theory allows us to explore the impact of line tension and the Poisson ratio on the assembly of curved surfaces. The method is general and may be generalized to surfaces without specific symmetries. In this way, the approach provides the first step towards obtaining a complete theory for the self assembly of nonspherical virus capsids.

The free energy of a partially formed elastic shell can be written as

$$F = F^{\text{elastic}} + F^{\text{bending}} + F^{\text{abs}} + F^{\text{line}}$$
$$= \int d^2\boldsymbol{x} \sqrt{g} [\mathcal{F}^{\text{elastic}} + \mathcal{F}^{\text{bending}}] + F^{\text{abs}} + F^{\text{line}}, \quad (1)$$

where the first and second terms correspond to the stretching and bending energies of the patch, respectively, the third term represents the attractive monomer-monomer interaction promoting the crystal growth, and the last term is associated with the cost of the rim energy due to the fact that the subunits at the boundary have fewer neighbors than the ones at the interior of the surface. The elastic term $\mathcal{F}^{\text{elastic}}$ [see Eq. (A1)] contains a quadratic term [29] in the strain tensor $u_{\alpha\beta}$

$$u_{\alpha\beta} = \frac{1}{2}[g_{\alpha\beta} - \bar{g}_{\alpha\beta}], \quad (2)$$

where $g_{\alpha\beta}(\boldsymbol{x})$ is the *actual metric* (the metric of the curved surface) and $\bar{g}_{\alpha\beta}(\bar{\boldsymbol{x}})$ is the *reference metric* describing a perfect lattice, i.e., the one consisting of equilateral triangles [Figs. 1(e)–1(h)]. Note that the Gaussian curvature of the reference metric is zero, except possibly, on a finite number of points that define disclination cores [25]. If a_L is the lattice constant of the perfect triangular lattice in reference space, the number of particles $N \gg 1$ making the crystal with a given area $\hat{A}$ is

$$\hat{A} = \int d^2\boldsymbol{x} \sqrt{g(\boldsymbol{x})} = \int d^2\bar{\boldsymbol{x}} \sqrt{\bar{g}(\bar{\boldsymbol{x}})} = \frac{\sqrt{3}}{2} Na_L^2. \quad (3)$$

The second term in Eq. (1) can be expressed in terms of the two radii of curvature $(R_i)_{i=1,2}$,

$$\mathcal{F}^{\text{bending}} = \kappa \left[\left(\frac{1}{R_1} - H_0 \right)^2 + \left(\frac{1}{R_2} - H_0 \right)^2 \right], \quad (4)$$

with κ the bending rigidity and H_0 the mean spontaneous curvature of the constituents or subunits. We emphasize that the free energy density, Eq. (1), has no trivial solution. The only surfaces allowing zero strains have either zero Gaussian curvature: a plane or cylinder ($q = 0$), or a delta function at the origin like a cone ($q = 1$). The absolute minimum of the bending rigidity implies a surface with $R_1 = R_2 = (1/H_0)$, a sphere. There is no surface that simultaneously minimizes both the elastic and bending energies. The third term in Eq. (1), $F^{\text{abs}} = -\Pi\hat{A} < 0$ with Π the attractive interaction per unit area due to favorable hydrophobic contacts between subunits, is the driving force for crystal growth [13].

In this Letter we consider a frozen geometry, so the actual metric $g_{\alpha\beta}(\boldsymbol{x})$ is that of the corresponding surface. The defect distribution is also given, so the reference metric $\bar{g}_{\alpha\beta}(\bar{\boldsymbol{x}})$ is fixed as well. The problem consists of mapping the actual and reference space $\boldsymbol{x} = \mathcal{U}(\bar{\boldsymbol{x}})$. In other words, $\mathcal{U}$ is the function that determines how the perfect lattice in reference space maps to the deformed one in actual space, as illustrated in Figs. 1(e)–1(h). For simplicity, in this Letter we consider only surfaces of revolution, defined by $x = r\cos(\theta)$, $y = r\sin(\theta)$, $z = f(r)$ with actual metric

$$ds^2 = [1 + f'(r)^2]dr^2 + r^2 d\theta^2, \quad (5)$$

see Fig. 1. Further, we consider an isotropic reference metric

$$ds^2 = \rho'(r)^2 dr^2 + \alpha^2 \rho(r)^2 d\theta^2 = d^2\rho + \alpha^2 \rho^2 d\theta^2 \quad (6)$$

with $\alpha = 1 - (q/6)$ and $q = 0, \pm 1$ corresponding to no disclination or with a disclination at the origin. The two metrics are basically *incompatible* [28], that is, for a fixed $f(r)$ there is no choice of $\rho(r)$ that will make the strain tensor Eq. (2) vanish, as their Gaussian curvatures generally differ. In the isotropic case, the function $\mathcal{U}$ describing the mapping from the actual to reference space (or reference to actual) can be expressed as $\rho(r)$ or $r(\rho)$. To make the presentation of the Letter simple, we consider a situation in which the surface is given through $f(r)$ (see Fig. 1). The elastic energy given in Eq. (1) depends on $\rho(r)$ and thus becomes Eq. (B1). And then the problem consists of finding the optimal $\rho(r)$ that minimizes the free energy Eq. (1). Following Refs. [25,27], this leads to

$$\nabla_\alpha \sigma^{\alpha\beta} + (\bar{\Gamma}^\beta_{\gamma\nu} - \Gamma^\beta_{\gamma\nu})\sigma^{\gamma\nu} = 0, \quad (7)$$

where $\sigma^{\alpha\beta}$ is the stress tensor and $\Gamma^\beta_{\gamma\nu}$ are the Christoffel symbols for the reference and actual metrics (see Appendix B). This is a one-dimensional nonlinear differential equation with just one unknown $\rho(r)$ (see Eq. (B6)). We solve Eq. (7) subject to the following boundary condition:

$$n_\rho \sigma^{\rho\lambda} \bar{g}_{\lambda\nu} = -\frac{\tau}{r_A} n_\nu, \quad (8)$$

where τ is the line tension, $n^\mu = g^{\mu\nu} n_\nu$ is the normal to the boundary within the surface, and r_A is the curvature of the boundary. For a surface with rotational symmetry and a circular boundary $r = r_0$, this equation simply becomes Eq. (C13). For a tensionless boundary, obviously $\tau = 0$. In Appendix C, we provide a detailed derivation of Eq. (8) from the line energy $F^{\text{line}} = \tau \oint_{\partial D} ds$ with ds an infinitesimal length for the boundary ∂D in actual space. We also show how Eqs. (1)–(8) reduce to standard linear elasticity and provide an explicit analytical solution within linear elasticity for both a spheroid, $f(r) = \beta\sqrt{R_0^2 - r^2}$ [Fig. 1(f)] and a sombrero surface, $f(r) = \beta R_0/3(1 - (r/R_0)^2 + (r/R_0)^4)^{3/2}$ [Fig. 1(h)], where β is a unitless number, in SM Sec. III.

To obtain the free energy of the system, we first calculate $\rho(r)$ through Eq. (7), which minimizes Eq. (1). The plots in Fig. 2 below each show the optimal $\rho(r)$ or $r(\rho)$ for both spheroid and sombrero surfaces with no disclination or with one disclination at the center. It is important to note that with the exact $r(\rho)$, we can reconstruct the lattice in actual space; the positions of the lattice in reference space $(\rho_i, \theta_i)_{i=1,\cdots N}$ are known and consist of N equilateral triangles with lattice constant a_L (if $N \gg 1$), see Eq. (3).
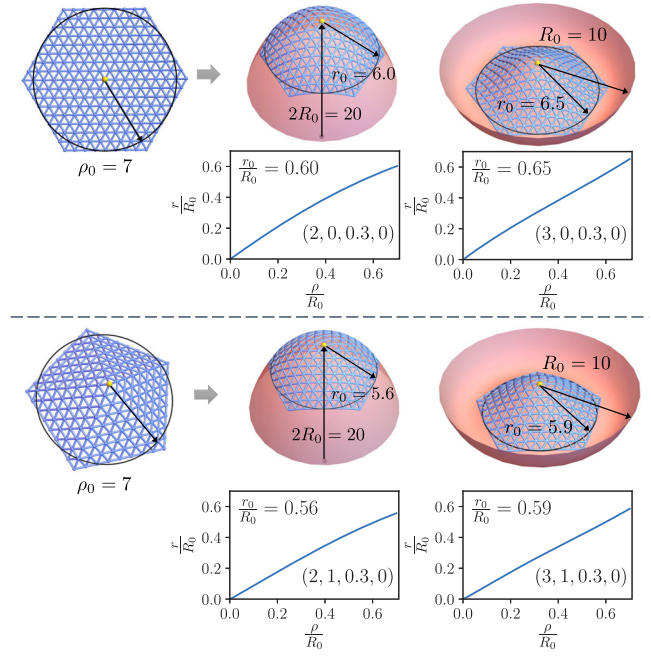

FIG. 2. Lattice reconstruction for both the spheroid and sombrero. The lengths R_0, ρ_0, and r_0 are given in units of the lattice constant a_L. The plots under spheroid and sombrero surfaces indicate the corresponding mapping function from the reference to actual space. $(\rho_0/R_0) = 0.7$ for each plot. The numbers in the parentheses in each figure denote $(\beta, q_i, \nu_p, \hat{\tau})$.

Then, from $r(\rho)$, the positions in actual space $[r(\rho_i), \theta_i]_{i=1,\cdots N}$ are obtained, as illustrated in Fig. 2. Thus, we find a solution to the problem of finding the best possible triangulation consisting of equilateral triangles that cover a given surface. Note that this solution is independent of the underlying potential among the constituent particles, and therefore, hereon we refer to this triangulation as the *universal mapping lattice*.

Plugging the solutions of $\rho(r)$ into Eq. (1), we obtain the free energy of the system. First, we consider the case of free boundary conditions as illustrated in Fig. 3. For comparison, we show the predictions from linear elasticity, which become exact in the limit of small curvature ($(\hat{A}/R_0^2) \to 0$), both for the defect free case $q_i = 0$ and a single disclination $q_i = 1$. Very generally, we find that the applicability of elasticity theory extends to relatively large curvatures ($(\hat{A}/R_0^2) \approx 1$). For the spheroid, linear elasticity remains qualitatively correct for the entire range explored, but this is not the case for the sombrero surface, see Fig. 3, where linear elasticity breaks down and cannot be extended beyond a certain limit.

The points where the $q_i = 0$ and $q_i = 1$ curves cross each other define whether it is energetically favorable to have a disclination at the center or not. The results are quoted in Table I. We compare with the most recent, and to our knowledge, most accurate predictions from Ref. [23]. Note that in some cases the differences are as high as 10%.
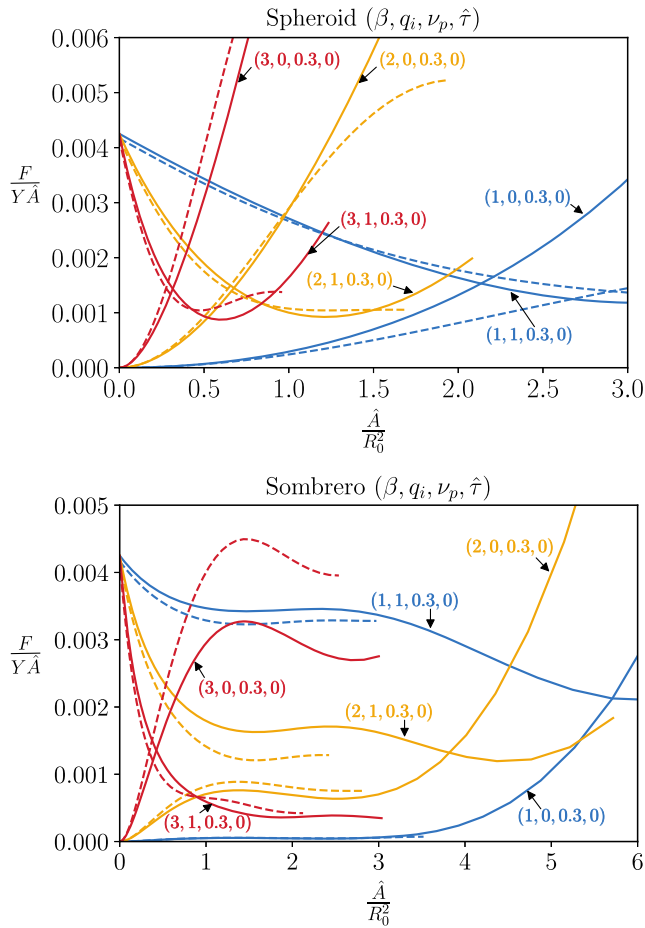
FIG. 3. Free energy for a spheroid and sombrero without ($q_i = 0$) and with ($q_i = 1$) a disclination at the center at $(\tau/YR_0) \equiv \hat{\tau} = 0$ (zero line tension) and at fixed Poisson ratio $\nu_p = 0.3$. The solid line corresponds to the exact results while the dashed line denotes the analytical results within linear elasticity. The three different colors represent different values of $\beta = 1, 2, 3$, indicating the magnitude of $f(r)$.

The case of a finite line tension is shown in Fig. 4. Basically, a large value of τ overshadows all the other energies of the system resulting into the collapse of all the free energy plots into an almost universal curve defined by the line tension term. The overall free energy is in some agreement with linear elasticity theory, which, as shown in the inset, is also true for the elastic contribution, see Eq. (1). In SM Sec. V, we provide similar plots for smaller values of the line tension (see Fig. S1).
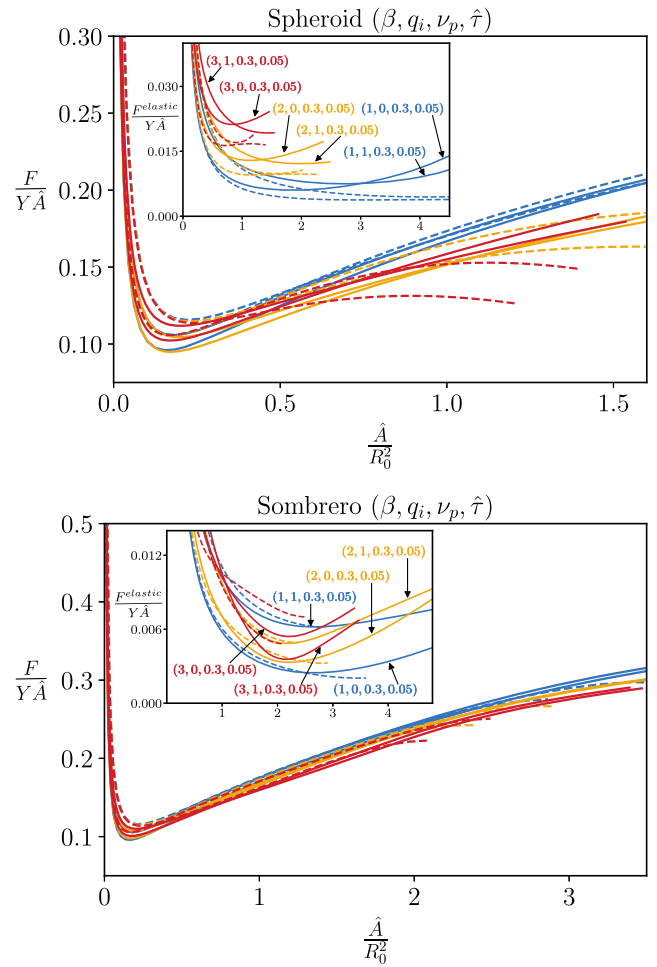
FIG. 4. Free energy [Eq. (1)] for both the spheroid and sombrero at finite line tension $(\tau/YR_0) = \hat{\tau} = 0.05$. The solid line corresponds to the exact results while the dashed line denotes the analytical results within linear elasticity.

In the absence of line tension, linear elasticity predicts that the free energy is a function of the Young modulus Y alone, independent of the Poisson ratio ν_p in SM Sec. III. This is implicitly assumed in models of interacting defects. Within the exact nonlinear theory presented in this Letter, we show that the dependence of the Poisson ratio at vanishing line tension is, indeed, negligible (see Fig. S2). However, Fig. 5 reveals that there is a dependence of the Poisson ratio whenever the line tension is nonzero, see also Fig. S2. We have been able to extract explicitly the

TABLE I. Transition points at which the surface with ($q_i = 1$) and without ($q_i = 0$) a disclination have the same energy. Here $\theta = (r/R_0)$ and θ_{AH} are the predictions reported in Ref. [23].

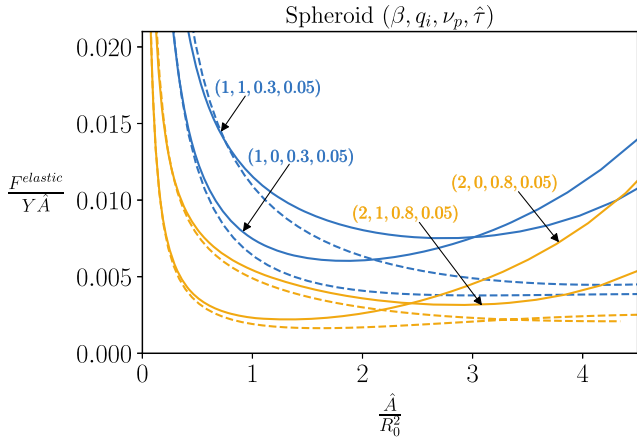|	$\beta = 1$			$\beta = 2$			$\beta = 3$		
	$(\hat{A}/R_0^2)$	θ	θ_{AH}	$(\hat{A}/R_0^2)$	θ	θ_{AH}	$(\hat{A}/R_0^2)$	θ	θ_{AH}
Spheroid	2.13	0.75	0.73	0.68	0.43	0.36	0.32	0.29	0.27
Sombrero	5.71	1.18	1.17	3.83	1.00	0.89	0.42	0.34	0.35

FIG. 5. The elastic energy [see Eq. (1)] for the spheroid at $(\tau/YR_0) = \hat{\tau} = 0.05$ for two different values of the Poisson ratio $\nu_p = 0.3$ and 0.8. The solid lines correspond to the exact results while the dashed lines denote analytical results within linear elasticity.

dependence of $\rho(r)$ or $r(\rho)$ on the Poisson ratio as the solution of the exact theory, see Figs. 2, S3, and S4.

As expected, for $(\hat{A}/R_0^2)$ small, the results are well described by linear elasticity, but as this value increases, they get progressively worse, and in the case of the sombrero, linear elasticity breaks down for sufficiently large values of $(\hat{A}/R_0^2)$.

In summary, this Letter provides an exact solution to the problem of determining the structure of crystals on a curved surface by formulating the problem in terms of geometric invariants, which besides connecting it to the well developed field of differential geometry of curves and surfaces, enables, what we believe, is a transparent interpretation of nonlinear elasticity theory. In addition, we show that effects that have been difficult to consider in the past, such as a finite line tension or dependence on the Poisson ration ν_p are easily included.

Our exact solution provides a *universal triangulation*, as shown in Fig. 2, that is, a solution to the problem of providing the optimal tiling of an arbitrary surface with triangles as close to equilateral as possible. In previous studies, determining particle positions requires numerical minimization methods, either through discretizations of elasticity theory [12,26,30] or using explicit potentials, most typically inverse power laws, on a sphere [20,31] and other geometries [32] as well. The problem with numerical minimizations is the cost and instabilities that appear for both a large number of particles N and/or complicated geometries. We note that our analytical approach does not suffer from any of these problems: it is independent of the number of particles N, see Eq. (3), and is stable for any differentiable surface.

The approach developed in this Letter allows us to understand how the pentameric defects appear and interact with each other with clear implications in viral shells,

specifically for the difficult cases of the assembly of nonspherical structures similar to those presented in Fig. 1. Determining the location of lattice defects in the growing shells with nonzero Gaussian curvature in the presence of boundaries with line tension for various values of Poisson ratio has been shown to be a very challenging task [33–36]. The theory developed here paves the path for tackling the problem of crystalline growth pathways. While in this Letter we restricted our study to a fixed geometry with a given number of particles and provided explicit solutions for problems with rotational symmetry, the approach is completely general for any geometry or number of disclinations, although its explicit description requires additional developments that will be provided in subsequent studies.

Appendix A: Explicit formulas.—In this Appendix, we provide explicit expressions for the formulas in the main text.

The explicit form of $\mathcal{F}^{\text{elastic}}$ is

$$\mathcal{F}^{\text{elastic}} = \frac{1}{2}A^{\alpha\beta\gamma\delta}u_{\alpha\beta}u_{\gamma\delta}, \quad (A1)$$

where $u_{\alpha\beta}$ [see Eq. (2) in the main text] is the strain tensor and

$$A^{\alpha\beta\gamma\delta} = \frac{Y}{1-\nu_p^2}[\nu_p g^{\alpha\beta}g^{\gamma\delta} + (1-\nu_p)g^{\alpha\gamma}g^{\beta\delta}], \quad (A2)$$

with Y the Young Modulus, ν_p the Poisson ratio, and $g^{\alpha\beta}$ the actual metric.

The Gaussian curvature is

$$K = \frac{\det(\partial_i\partial_j f)}{[1+(\nabla f)^2]} = \frac{f'(r)f''(r)}{r[1+f'(r)^2]^2}, \quad (A3)$$

and the mean curvature (with the convention that $R_i = R > 0$, $i = 1, 2$ for the sphere) is

$$2H = -\nabla \cdot \left(\frac{\nabla f}{[1+(\nabla f)^2]^{1/2}}\right)$$
$$= -\left(\frac{f''(r)}{[1+f'(r)^2]^{3/2}} + \frac{f'(r)}{r[1+f'(r)^2]^{1/2}}\right), \quad (A4)$$

see Ref. [11] for the details. The two curvatures can be obtained from the equation

$$K = \frac{1}{R_1 R_2}$$

$$2H = \frac{1}{R_1} + \frac{1}{R_2}, \quad (A5)$$

such that $(1/R_1) = H + \sqrt{H^2 - K}$ and $(1/R_2) = H - \sqrt{H^2 - K}$ with H and K given in Eqs. (A3) and (A4). The stress tensor is

$$\sigma^{\alpha\beta} = \frac{1}{\sqrt{g}} \frac{\delta F}{\delta u_{\alpha\beta}} = A^{\alpha\beta\gamma\delta} u_{\gamma\delta}. \qquad (A6)$$

Appendix B: Surfaces of revolution.—In this section, we provide various quantities for the surfaces of revolution, defined by $x = r\cos(\theta)$, $y = r\sin(\theta)$, $z = f(r)$ with actual metric defined in Eq. (5).

The nonzero Christoffel symbols are given in Ref. [25] and are

symbol	Γ^r_{rr}	$\Gamma^r_{\theta\theta}$	$\Gamma^\theta_{\theta r}$
reference	$\dfrac{\rho''(r)}{\rho'(r)}$	$-\alpha^2 \dfrac{\rho(r)}{\rho'(r)}$	$\dfrac{\rho'(r)}{\rho(r)}$
actual	$\dfrac{f'(r)f''(r)}{1+f'(r)^2}$	$\dfrac{-r}{1+f'(r)^2}$	$\dfrac{1}{r}$.

The elastic energy given in Eq. (1) depends on $\rho(r)$,

$$\frac{F^{\text{elastic}}}{Y\pi} = \frac{1}{4(1-\nu_p^2)} \int dr\, r(1+f'(r)^2)^{1/2}$$
$$\times \left[\left(1 - \frac{\rho'(r)^2}{1+f'(r)^2}\right)^2 + \left(1 - \frac{\alpha^2\rho(r)^2}{r^2}\right)^2 \right.$$
$$\left. + 2\nu_p \left(1 - \frac{\rho'(r)^2}{1+f'(r)^2}\right)\left(1 - \frac{\alpha^2\rho(r)^2}{r^2}\right) \right]. \quad (B1)$$

The stress tensor given in Eq. (A6) becomes

$$\sigma^{rr} = \frac{Y}{2(1-\nu_p^2)(1+f'(r)^2)} \left\{ 1 - \frac{\rho'(r)^2}{1+f'(r)^2} \right.$$
$$\left. + \nu_p \left[1 - \left(\frac{\alpha\rho(r)}{r}\right)^2 \right] \right\}$$

$$\sigma^{r\theta} = \sigma^{\theta r} = 0$$

$$\sigma^{\theta\theta} = \frac{Y}{2r^2(1-\nu_p^2)} \left[\nu_p \left(1 - \frac{\rho'(r)^2}{1+f'(r)^2}\right) + 1 - \left(\frac{\alpha\rho(r)}{r}\right)^2 \right]. \qquad (B2)$$

Using Eq. (B1) and Eq. (B2), the general form of Eq. (7) for $\beta = r$ becomes

$$\partial_r \sigma^{rr} + \bar{\Gamma}^r_{rr}\sigma^{rr} + \bar{\Gamma}^r_{rr}\sigma^{rr} + \bar{\Gamma}^r_{\theta\theta}\sigma^{\theta\theta} + \Gamma^r_{rr}\sigma^{rr} + \Gamma^\theta_{\theta r}\sigma^{rr} = 0, \quad (B3)$$

which can be written as

$$\frac{d\sigma^{rr}}{dr} + (\bar{\Gamma}^r_{rr} + \Gamma^r_{rr} + \Gamma^\theta_{\theta r})\sigma^{rr} + \bar{\Gamma}^r_{\theta\theta}\sigma^{\theta\theta} = 0. \quad (B4)$$

The explicit form of the derivative of the stress tensor is

$$\frac{d\sigma^{rr}}{dr} = \frac{-Y}{(1-\nu_p^2)} \frac{f'(r)f''(r)}{(1+f'(r)^2)^2} \left\{ 1 - \frac{\rho'(r)^2}{1+f'(r)^2} \right.$$
$$\left. + \nu_p \left[1 - \left(\frac{\alpha\rho(r)}{r}\right)^2 \right] \right\}$$
$$+ \frac{Y}{(1-\nu_p^2)[1+f'(r)^2]} \left[\frac{\rho'(r)^2 f'(r)f''(r)}{[1+f'(r)^2]^2} \right.$$
$$\left. - \frac{\rho'(r)\rho''(r)}{1+f'(r)^2} + \nu_p \frac{\alpha^2\rho(r)^2}{r^3} - \nu_p \frac{\alpha^2\rho(r)\rho'(r)}{r^2} \right]. \quad (B5)$$

The equation determining $\rho(r)$, Eq. (B4), becomes

$$\frac{-f'(r)f''(r)}{(1+f'(r)^2)} \left\{ 1 - \frac{\rho'(r)^2}{1+f'(r)^2} + \nu_p \left[1 - \left(\frac{\alpha\rho(r)}{r}\right)^2 \right] \right\} + \frac{1}{1+f'(r)^2} \times \left[\frac{\rho'(r)^2 f'(r)f''(r)}{[1+f'(r)^2]^2} - \frac{\rho'(r)\rho''(r)}{1+f'(r)^2} + \nu_p \frac{\alpha^2\rho(r)^2}{r^3} \right.$$
$$\left. - \nu_p \frac{\alpha^2\rho(r)\rho'(r)}{r^2} \right] + \left(\frac{\rho''(r)}{\rho'(r)} + \frac{f'(r)f''(r)}{1+f'(r)^2} + \frac{1}{r} \right) \times \frac{1}{2[1+f'(r)^2]} \left\{ 1 - \frac{\rho'(r)^2}{1+f'(r)^2} + \nu_p \left[1 - \left(\frac{\alpha\rho(r)}{r}\right)^2 \right] \right\}$$
$$- \frac{\alpha^2\rho(r)}{2r^2\rho'(r)} \times \left[\nu_p \left(1 - \frac{\rho'(r)^2}{1+f'(r)^2}\right) + 1 - \left(\frac{\alpha\rho(r)}{r}\right)^2 \right] = 0. \qquad (B6)$$

Appendix C: Boundary conditions.—The boundary conditions can be obtained through the variations of $F^{\text{area}} = F^{\text{elastic}} + F^{\text{bending}}$ in Eq. (1) and the reparameterizations of the actual metric,

$$\delta F^{\text{area}} = -\int d^2 x \partial_\rho(\sqrt{g}\sigma^{\rho\mu}\bar{\xi}_\mu) = \oint \sqrt{g} dx^\mu \varepsilon_{\mu\nu}\sigma^{\nu\rho}\bar{\xi}_\rho. \quad (C1)$$

If there is a line tension τ, the contribution to the free energy is then

$$F^{\text{line}} = \tau \oint ds = \tau \oint \sqrt{\langle g \rangle} dl = \tau \oint dx^\mu g_{\mu\nu} t^\nu, \quad (C2)$$

where $\langle g \rangle = g_{\mu\nu}(dx^\mu/dl)(dx^\nu/dl)$ and

$$t^\mu = \frac{1}{\sqrt{\langle g \rangle}} \frac{dx^\mu}{dl} \qquad (C3)$$

is the unit vector (in the actual metric) tangent to the boundary curve with $dx^\mu = \sqrt{\langle g \rangle} t^\mu dl$. The variations to the free energy Eq. (C2) as shown in Ref. [25] then become

$$\delta F^{\text{line}} = \frac{\tau}{2} \oint dx^\mu \delta g_{\mu\nu} t^\nu = -\tau \oint dx^\mu \nabla_\mu \xi_\nu t^\nu$$

$$= \tau \oint dx^\mu \xi_\nu \nabla_\mu t^\nu. \qquad (C4)$$

Since $\delta(F^{\text{area}} + F^{\text{line}}) = 0$, the appropriate boundary condition is then

$$\tau g_{\rho\nu} \nabla_\mu t^\rho = -\sqrt{g} \epsilon_{\mu\rho} \sigma^{\rho\lambda} \bar{g}_{\lambda\nu}. \qquad (C5)$$

Note the tangent vector is

$$t^\rho \nabla_\rho t^\mu = -\frac{1}{r_A} n^\mu, \qquad (C6)$$

where r_A is the curvature of the curve defining the boundary. The normal to the tangent vector can be written as

$$n_\mu = \sqrt{g} \epsilon_{\mu\rho} t^\rho. \qquad (C7)$$

The boundary condition, thus, becomes

$$n_\rho \sigma^{\rho\lambda} \bar{g}_{\lambda\nu} = -\frac{\tau}{r_A} n_\nu. \qquad (C8)$$

This condition is slightly different from the one given in Ref. [25]. This is because $\xi^\mu = \bar{\xi}^\mu$ so that $g_{\mu\nu} \xi^\nu = \xi_\mu \neq \bar{\xi}_\mu = \bar{g}_{\mu\nu} \xi^\nu$, which was overlooked in previous work.

As an example, if the problem has rotational symmetry and the boundary is a circle $r = r_0$, then $\theta(s) = s/r_0$. The tangent vectors then are

$$t^r = 0 \qquad t^\theta = \frac{1}{r_0}, \qquad (C9)$$

and the normal vectors

$$n_r = \sqrt{1 + f'(r_0)^2} \qquad n_\theta = 0. \qquad (C10)$$

Then Eq. (C6) becomes

$$t^\rho \nabla_\rho t^r = \Gamma^r_{\theta\theta} \frac{1}{r_0^2} = -\frac{1}{r_0[1 + f'(r_0)^2]}$$
$$= -\frac{1}{r_0 \sqrt{1 + f'(r_0)^2}} n^r \qquad (C11)$$

with

$$\frac{r_A}{r_0} = \sqrt{1 + f'(r_0)^2}. \qquad (C12)$$

Finally, the boundary condition becomes equal to

$$\bar{g}_{rr}(r_0) \sigma^{rr}(r_0) = -\frac{1}{\sqrt{1 + f'(r_0)^2}} \frac{\tau}{r_0}. \qquad (C13)$$

For a sphere $f'(r) = -[r/(\sqrt{R_0^2 - r^2})]$ and thus

$$r_A = \frac{r_0}{\sqrt{1 - \left(\frac{r_0}{R_0}\right)^2}}. \qquad (C14)$$

[1] M. F. Hagan, Modeling viral capsid assembly, Adv. Chem. Phys. **155**, 1 (2014).

[2] R. F. Garmann, M. Comas-Garcia, C. M. Knobler, and W. M. Gelbart, Physical principles in the self-assembly of a simple spherical virus, Acc. Chem. Res. **49**, 48 (2016).

[3] R. Twarock and A. Luque, Structural puzzles in virology solved with an overarching icosahedral design principle, Nat. Commun. **10**, 4414 (2019).

[4] S. Panahandeh, S. Li, and R. Zandi, The equilibrium structure of self-assembled protein nano-cages, Nanoscale **10**, 22802 (2018).

[5] S. Panahandeh, S. Li, L. Marichal, R. Leite Rubim, G. Tresset, and R. Zandi, How a virus circumvents energy barriers to form symmetric shells, ACS Nano **14**, 3170 (2020).

[6] F. Mohajerani and M. F. Hagan, The role of the encapsulated cargo in microcompartment assembly, PLoS Comput. Biol. **14**, e1006351 (2018).

[7] Z. H. Zhou, M. Dougherty, J. Jakana, J. He, F. J. Rixon, and W. Chiu, Seeing the herpesvirus capsid at 8.5 å, Science **288**, 877 (2000).

[8] B. K. Ganser, S. Li, V. Y. Klishko, J. T. Finch, and W. I. Sundquist, Assembly and analysis of conical models for the hiv-1 core, Science **283**, 80 (1999).

[9] S. Li, P. Roy, A. Travesset, and R. Zandi, Why large icosahedral viruses need scaffolding proteins, Proc. Natl. Acad. Sci. U.S.A. **115**, 10971 (2018).

[10] J. Ning, G. Erdemci-Tandogan, E. L. Yufenyuy, J. Wagner, B. A. Himes, G. Zhao, C. Aiken, R. Zandi, and P. Zhang, In vitro protease cleavage and computer simulations reveal the hiv-1 capsid maturation pathway, Nat. Commun. **7**, 13689 (2016).

[11] R. Zandi, B. Dragnea, A. Travesset, and R. Podgornik, On virus growth and form, Phys. Rep. **847**, 1 (2020).

[12] H. S. Seung and D. R. Nelson, Defects in flexible membranes with crystalline order, Phys. Rev. A **38**, 1005 (1988).

[13] A. Y. Morozov and R. F. Bruinsma, Assembly of viral capsids, buckling, and the Asaro-Grinfeld-Tiller instability, Phys. Rev. E **81**, 041925 (2010).

[14] A. Azadi and G. M. Grason, Emergent Structure of Multi-dislocation Ground States in Curved Crystals, Phys. Rev. Lett. **112**, 225502 (2014).

[15] G. M. Graison, Colloquium: Geometry and optimal packing of twisted columns and filaments, Rev. Mod. Phys. **87**, 401 (2015).

[16] M. Castelnovo, Viral self-assembly pathway and mechanical stress relaxation, Phys. Rev. E **95**, 052405 (2017).

[17] A. Košmrlj and D. R. Nelson, Statistical Mechanics of Thin Spherical Shells, Phys. Rev. X **7**, 011002 (2017).

[18] A. Pérez-Garrido, M. J. W. Dodgson, and M. A. Moore, Influence of dislocations in Thomson's problem, Phys. Rev. B **56**, 3640 (1997).

[19] M. J. Bowick, D. R. Nelson, and A. Travesset, Interacting topological defects on frozen topographies, Phys. Rev. B **62**, 8738 (2000).

[20] M. Bowick, A. Cacciuto, D. R. Nelson, and A. Travesset, Crystalline Order on a Sphere and the Generalized Thomson Problem, Phys. Rev. Lett. **89**, 185502 (2002).

[21] J. Lidmar, L. Mirny, and D. R. Nelson, Virus shapes and buckling transitions in spherical shells, Phys. Rev. E **68**, 051910 (2003).

[22] L. Giomi and M. Bowick, Crystalline order on Riemannian manifolds with variable Gaussian curvature and boundary, Phys. Rev. B **76**, 054106 (2007).

[23] S. Agarwal and S. Hilgenfeldt, Simple, General Criterion for Onset of Disclination Disorder on Curved Surfaces, Phys. Rev. Lett. **125**, 078003 (2020).

[24] See Supplemental Material at http://link.aps.org/supplemental/10.1103/PhysRevLett.129.088001 for details on Mathematica notebooks for connection with linear elasticity theory, free energy normalization, units, and additional plots.

[25] S. Li, R. Zandi, and A. Travesset, Elasticity in curved topographies: Exact theories and linear approximations, Phys. Rev. E **99**, 063005 (2019).

[26] S. Li, R. Zandi, A. Travesset, and G. M. Grason, Ground States of Crystalline Caps: Generalized Jellium on Curved Space, Phys. Rev. Lett. **123**, 145501 (2019).

[27] E. Efrati, E. Sharon, and R. Kupferman, Elastic theory of unconstrained non-Euclidean plates, J. Mech. Phys. Solids **57**, 762 (2009).

[28] M. Moshe, E. Sharon, and R. Kupferman, Elastic interactions between two-dimensional geometric defects, Phys. Rev. E **92**, 062403 (2015).

[29] L. Landau and E. M. Lifshitz, *Theory of Elasticity*, 3rd ed. (Butterworth-Heinemann, London, 1985).

[30] A. Travesset, Universality in the screening cloud of dislocations surrounding a disclination, Phys. Rev. B **68**, 115421 (2003).

[31] A. Pérez-Garrido, M. Ortuño, E. Cuevas, and J. Ruiz, Many-particle jumps algorithm and Thomson's problem, J. Phys. A **29**, 1973 (1996).

[32] E. Bendito, M. J. Bowick, A. Medina, and Z. Yao, Crystalline particle packings on constant mean curvature (Delaunay) surfaces, Phys. Rev. E **88**, 012405 (2013).

[33] R. F. Garmann, A. M. Goldfain, and V. N. Manoharan, Measurements of the self-assembly kinetics of individual viral capsids around their rna genome, Proc. Natl. Acad. Sci. U.S.A. **116**, 22485 (2019).

[34] M. Chevreuil, D. Law-Hine, J. Chen, S. Bressanelli, S. Combet, D. Constantin, J. Degrouard, J. Möller, M. Zeghal, and G. Tresset, Nonequilibrium self-assembly dynamics of icosahedral viral capsids packaging genome or polyelectrolyte, Nat. Commun. **9**, 3071 (2018).

[35] E. C. Dykeman, P. G. Stockley, and R. Twarock, Solving a Levinthal's paradox for virus assembly identifies a unique antiviral strategy, Proc. Natl. Acad. Sci. U.S.A. **111**, 5361 (2014).

[36] S. Panahandeh, S. Li, B. Dragnea, and R. Zandi, Virus assembly pathways inside a host cell, ACS Nano **16**, 317 (2022).